

UNIT project: Universe N -body simulations for the Investigation of Theoretical models from galaxy surveys

Chia-Hsun Chuang^{1*}, Gustavo Yepes^{2,3†}, Francisco-Shu Kitaura^{4,5}, Marcos Pellejero-Ibanez^{4,5}, Sergio Rodríguez-Torres^{2,3}, Yu Feng⁶, R. Benton Metcalf^{7,8}, Risa H. Wechsler^{1,9,10}, Cheng Zhao^{11,12}, Chun-Hao To^{1,9,10}, Shadab Alam¹³, Arka Banerjee^{1,9,10}, Joseph DeRose^{1,9,10}, Carlo Giocoli^{8,14,7,15}, Alexander Knebe^{2,3,16}, Guillermo Reyes^{2,3}

¹*Kavli Institute for Particle Astrophysics and Cosmology, Stanford University, 452 Lomita Mall, Stanford, CA 94305, USA*

²*Departamento de Física Teórica, Módulo 8, Facultad de Ciencias, Universidad Autónoma de Madrid, 28049 Madrid, Spain*

³*CIAFF, Facultad de Ciencias, Universidad Autónoma de Madrid, 28049 Madrid, Spain*

⁴*Instituto de Astrofísica de Canarias (IAC), C/Vía Láctea, s/n, E-38200, La Laguna, Tenerife, Spain*

⁵*Departamento Astrofísica, Universidad de La Laguna (ULL), E-38206 La Laguna, Tenerife, Spain*

⁶*Berkeley Center for Cosmological Physics, Department of Physics, University of California Berkeley, Berkeley CA, 94720, USA*

⁷*Dipartimento di Fisica e Astronomia, Alma Mater Studiorum Università di Bologna, via Gobetti 93/2, I-40129 Bologna, Italy*

⁸*INAF - Osservatorio di Astrofisica e Scienza dello Spazio di Bologna, via Gobetti 93/3, I-40129 Bologna, Italy*

⁹*Department of Physics, Stanford University, 382 Via Pueblo Mall, Stanford, CA 94305, USA*

¹⁰*SLAC National Accelerator Laboratory, 2575 Sand Hill Road, Menlo Park, CA 94025, USA*

¹¹*Laboratoire d'Astrophysique, Ecole Polytechnique Fédérale de Lausanne (EPFL), Observatoire de Sauverny, CH-1290 Versoix, Switzerland*

¹²*National Astronomical Observatories, Chinese Academy of Science, Beijing 100012, P.R.China*

¹³*Institute for Astronomy, University of Edinburgh, Royal Observatory, Blackford Hill, Edinburgh, EH9 3HJ, UK*

¹⁴*Dipartimento di Fisica e Scienze della Terra, Università degli Studi di Ferrara, via Saragat 1, I-44122 Ferrara, Italy*

¹⁵*INFN - Sezione di Bologna, viale Berti Pichat 6/2, I-40127 Bologna, Italy*

¹⁶*ICRAR, University of Western Australia, 35 Stirling Highway, Crawley, Western Australia 6009, Australia*

Accepted XXX. Received YYY; in original form ZZZ

ABSTRACT

We present the UNIT N -body cosmological simulations project, which is designed to provide precise predictions for nonlinear statistics of the galaxy distribution appropriate for characterizing emission line and luminous red galaxies in the current and upcoming generation of galaxy surveys. We investigate the recently suggested technique of Angulo & Pontzen 2016 designed to suppress the variance of cosmological simulations with a suite of precise particle mesh simulations (FastPM) as well as with full N -body calculations with a mass resolution of $\sim 1.2 \times 10^9 h^{-1} M_{\odot}$. We study redshift space distortions, cosmic voids, higher order statistics from $z = 2$ down to $z = 0$. We find that both two- and three-point statistics are unbiased, and that over the scales of interest for baryon acoustic oscillations and redshift-space distortions, the variance is greatly reduced in the two-point statistics and in the cross correlation between halos and cosmic voids, but is not reduced significantly for the three-point statistics. We demonstrate that the accuracy of the two-point correlation function for a galaxy survey having an effective volume of $20 (h^{-1} \text{Gpc})^3$ is improved by about a factor of 40, meaning that two pairs of simulations with a volume of $1 (h^{-1} \text{Gpc})^3$ lead to the equivalent variance of ~ 150 such simulations. The N -body simulations presented here thus provide an effective survey volume of about seven times the effective survey volume of DESI or Euclid. The data from this project, including dark matter fields, halo catalogues, and their clustering statistics, are publicly available at: <http://www.unitsims.org>.

Key words: large-scale structure of the Universe, N -body simulations

* E-mail: chuangch@stanford.edu

† E-mail: gustavo.yepes@uam.es

1 INTRODUCTION

The large-scale structure measured in galaxy surveys represents one of the most powerful probes of present day cosmology and of the nature of dark matter and dark energy in the Universe. To this end, a considerable observational effort is being put forward to map the three dimensional galaxy distribution in the Universe at unprecedented scales by means of large photometric and spectroscopic surveys that will measure the positions of millions of galaxies. The number and scale of galaxy surveys is dramatically increasing; the current largest are the photometric Dark Energy Survey¹ (DES) and the Extended Baryon Oscillation Spectroscopic Survey² (eBOSS). There are several large upcoming ground- and space-based experiments, including as 4MOST³ (4-metre Multi-Object Spectroscopic Telescope, [de Jong et al. 2012](http://www.4most.eu/)), DESI⁴ (Dark Energy Spectroscopic Instrument, [Schlegel et al. 2011](http://desi.lbl.gov/); [Levi et al. 2013](http://desi.lbl.gov/)), HETDEX⁵ (Hobby-Eberly Telescope Dark Energy Experiment, [Hill et al. 2008](http://hetdex.org/)), J-PAS⁶ (Javalambre Physics of accelerating universe Astrophysical Survey, [Benitez et al. 2014](http://j-pas.org/)), PFS⁷ (Subaru Prime Focus Spectrograph, [Takada et al. 2014](http://pfs.ipmu.jp/)), LSST⁸ (Large Synoptic Survey Telescope, [Abell et al. 2009](http://www.lsst.org/lsst/)), Euclid⁹ ([Laureijs et al. 2011](http://www.euclid-ec.org/)), and WFIRST¹⁰ (Wide-Field Infrared Survey Telescope, [Spergel et al. 2013](http://wfirst.gsfc.nasa.gov/)).

In order to robustly extract cosmological constraints from these surveys, we need to be sure that the potential systematic error from theoretical models, that for example characterize the galaxy power spectrum or correlation function as a function of cosmological model, is well below the statistical uncertainties caused by cosmic variance and shot noise. Some pioneering analytical models have been developed to compute the theoretical expected correlation function. To date, these models have limited accuracy, as they rely on analytical gravity models (e.g. [Zel'dovich 1970](http://www.zel'dovich.org/)), simplified biasing descriptions, and approximate redshift-space distortion models (see [White 2015](http://www.white2015.org/), and references therein). These models have not achieved the accuracy possible with a numerical computation using a full gravity solver. To meet the goals of current galaxy surveys we would need to run simulations with much larger effective volumes than those probed by the surveys *and* with enough mass resolution to resolve the dark matter halos hosting the typical galaxies detected in those surveys. Yet, the computational resources needed to accomplish this task are at the edge of the current (petaflop) computational power. One simulation with the required halo mass resolution ($\sim 4 \times 10^{11} h^{-1} M_{\odot}$, [Cochrane et al. 2017](http://www.cochrane2017.org/)) that covers the whole volume sampled by Euclid ($\sim 70 \text{ Gpc}^3$) would demand an enormous number of particles (more than $16,000^3$ in a $4 \text{ Gpc} h^{-1}$ box). The largest N -body simulations, e.g., MillenniumXXL ([Angulo et al. 2012](http://www.millenniumxxl.org/)),

MICE ([Fosalba et al. 2015](http://www.fosalba2015.org/)), MultiDark ([Klypin et al. 2016](http://www.klypin2016.org/)), Dark Sky ([Skillman et al. 2014](http://www.skillman2014.org/)), OuterRim ([Habib et al. 2016](http://www.habib2016.org/)), FLAGSHIP ([Potter et al. 2016](http://www.potter2016.org/)), performed so far are still well below this particle number despite their computational expense.

In this project, we explore an alternative way of reaching the same level of required accuracy using far fewer computational resources. Recently, [Angulo & Pontzen \(2016\)](http://www.angulo2016.org/) proposed a new method to dramatically reduce cosmic variance arising from the sparse sampling of small wave modes in cosmological simulations. The method uses pairs of simulations ([Pontzen et al. 2016](http://www.pontzen2016.org/)) with initial Fourier-mode amplitudes that are fixed to the ensemble-averaged power spectrum, with initial modes that are exactly out of phase (one of the pair of simulations has opposite phases with respect to its companion). Using this methodology, one can potentially obtain a result that is statistically equivalent to the mean of many independent simulations from just a pair of simulations.

To date, the method has been tested only on the dark matter distribution at high redshifts ($z = 1$) obtained with particle mesh gravity solvers, with a low-resolution particle mass of $1.7 \times 10^{12} h^{-1} M_{\odot}$. Given that fixed initial conditions cease to be formally a Gaussian field with a fixed power spectrum, there was some concern about potential biases this approach could introduce in the clustering statistics, although [Angulo & Pontzen \(2016\)](http://www.angulo2016.org/) gave analytical arguments why the biases should be negligible. [Villaescusa-Navarro et al. \(2018\)](http://www.villaescusa2018.org/) further tested this method using hydrodynamical simulations. These simulations were done with small volumes ($20 h^{-1} \text{ Mpc}$ side) or with low resolutions (particle mass of $6.6 \times 10^{11} h^{-1} M_{\odot}$) compared to the requirements of current and upcoming surveys.

There is a need to directly test the usefulness and applicability of this approach to key large-scale structure analyses, including baryon acoustic oscillations and redshift-space distortions, that are expected with upcoming large surveys. That is the goal of the present work. Here, we extend these studies to the statistics, redshift range, galaxy samples, resolution, and volume required by surveys such as DESI and Euclid. We use volumes of $(h^{-1} \text{ Gpc})^3$ in our studies. Such volumes have been claimed to be large enough to account for large-scale mode coupling ([Klypin & Prada 2018](http://www.klypin2018.org/)), although this likely needs to be further investigated; missing modes may need to be accounted for in a post-processing step ([Chuang et al in prep](http://www.chuang2018.org/)).

We have designed the simulations in the present work to robustly model the expected halo masses for emission line galaxies (ELGs) ($\sim 10^{11} h^{-1} M_{\odot}$, [González-Pérez et al. 2018](http://www.gonzalez2018.org/)) and H α galaxies ($\sim 4 \times 10^{11} h^{-1} M_{\odot}$, [Cochrane et al. 2017](http://www.cochrane2017.org/)). The simulation boxes are $1 h^{-1} \text{ Gpc}$ on a side, with 4096^3 particles and a mass resolution of $1.2 \times 10^9 h^{-1} M_{\odot}$. We are thus able to safely resolve all halos with masses larger than $1.2 \times 10^{11} h^{-1} M_{\odot}$ (using 100 particles per halo).

We demonstrate that the resulting errors in the statistical correlation function measurements using the suppressed variance method are equivalent to having more than 7 times the effective volume of the Universe sampled by DESI or Euclid galaxies ($\sim 20 (h^{-1} \text{ Gpc})^3$). We generate halo catalogs and merger trees, using the publicly available ROCKSTAR halo finder ([Behroozi et al. 2013a](http://www.behroozi2013a.org/)), together with density and velocity fields on a mesh for later construction of light cone dis-

¹ <http://www.darkenergysurvey.org>

² <http://www.sdss.org/sdss-surveys/eboss/>

³ <http://www.4most.eu/>

⁴ <http://desi.lbl.gov/>

⁵ http://hetdex.org

⁶ http://j-pas.org

⁷ <https://pfs.ipmu.jp>

⁸ <http://www.lsst.org/lsst/>

⁹ <http://www.euclid-ec.org>

¹⁰ <http://wfirst.gsfc.nasa.gov>

tributions of galaxies and weak lensing maps. In future work, we will use these simulations to produce thousands of catalogs, including mock galaxies with various techniques. The corresponding data will be made publicly available through databases and web portals for the general use of the astrophysical community¹¹.

This paper is organized as follows. First we present our study of the potential systematic biases from Suppressed Variance Methods (hereafter SVM) (Section 2). In Section 3, we present our suppressed variance simulation products including a clustering analysis and a robust assessment of the improvement. We summarize and conclude in Section 4. Throughout this work we use the following cosmological parameter: $\Omega_m = 0.3089$, $h \equiv H_0/100 = 0.6774$, $n_s = 0.9667$ and $\sigma_8 = 0.8147$ (see Table 4 in Planck Collaboration XIII et al. 2016).

2 ASSESMENT OF POTENTIAL SYSTEMATIC BIASES IN SVM

We begin by studying the potential systematic biases and the improvement introduced by the suppressed variance method. To this end, we want to generate a large total volume and number of simulations that permit us to estimate the uncertainties of the measurements and to quantify the improvements in the error bars in different clustering measurements.

To create large simulated volumes, we rely on accelerated particle-mesh solvers, which have been recently shown to produce accurate halo populations compared to full N -body calculations, when enhanced with various techniques (see the COLA code Tassev et al. 2013 or the FastPM code Feng et al. 2016).

2.1 Setup

We use the C implementation FastPM software, which uses a pencil domain-decomposition in the Poisson solver for gravity; a Fourier-space four-point differential kernel is used to compute the force. The time integration scheme is modified from vanilla leap-frog to account for acceleration of velocity during a step and thus to correctly track the linear growth of large-scale modes regardless of the number of time steps.

This permits us to efficiently perform 800 paired simulations to benchmark the method. Half of them (400) have low resolution (1024^3 particles), but large volume ($1 h^{-1}$ Gpc side), and the other half (400) have enough resolution for the purpose of this study (1024^3 particles, see Section 3), but smaller volume ($250 h^{-1}$ Mpc side). In each case we run half of the paired simulations with normal half with fixed amplitudes, yielding 100 pair simulations for each case (see Table 1).

The simulations are started at $a \equiv 1/(1+z) = 0.01$ ($z = 99$), and evolved to $a = 1$ ($z = 0$) with 100 timesteps. The redshift of the output boxes we save are $z = 2$, $z = 1$ and $z = 0$. These regular simulation sets in high and low resolution define our reference simulations (see Table 1), from which we compute the standard mean summary statistics.

¹¹ see <http://www.unitsims.org>

When computing halos with the Friends-of-Friends halo finder in `nbodykit` (Hand et al. 2017), we choose a minimum of 20 dark matter particles per halo and a linking length of $0.2 L_{\text{box}}/N_c$. Here L_{box} refers to the size of one side of the simulation box and N_c to the number of cells used in the mesh computation, which was taken to correspond to the number of dark matter particles.

The different sets of simulations are illustrated in the density maps from the $1 h^{-1}$ Gpc side boxes sharing the same seed, as can be seen in Fig. 1. The maps correspond to boxes of normal pairs (regular and inverse phase) and fixed-amplitude pairs. Although the fixed amplitude map shows a slightly different density distribution as compared to the regular one, there are no prominent features distinguishable by eye between the maps. This represents a first rough indication that the statistics of the simulations with SVM remain valid. This requires, however, a proper inspection, as we will present and discuss in the following sections.

2.2 Results from particle mesh simulations

We perform an analysis of several different clustering statistics, including the power spectrum (PK), correlation function (CF), and bispectrum (BK) (as defined for instance in Chuang et al. 2017) using dark matter particles and halos based on the set of fast particle mesh simulations. We demonstrate below that there are no systematic biases using the SVM, and that the variance is indeed greatly reduced in two-point statistics over the scales of interest to BAO and RSD analysis.

We quantify these measurements through the standard deviation of the reference simulations: $\sigma_{\text{ref}}(k)$, and the deviation of the mean with respect to the reference mean: $\Delta(k)$. The top panels in Figs. 2 and 3 show the original comparison of the clustering statistics; the middle panels show the comparison of the mean normalized by the uncertainty of the reference LR 100 boxes. Since the uncertainty on the mean should be inversely proportional to $\sqrt{100}$, deviations between the means should be considered as unbiased if they agree within $0.1\sigma_{\text{ref}}$. This study is performed for dark matter particles, halos, and cosmic voids, as we discuss below.

2.2.1 dark matter particles

The largest suppression of variance is obtained for the dark matter particles. Fig. 2 shows the comparison of the dark matter particle clustering measurements from FastPM runs with $1 h^{-1}$ Gpc side boxes and 1024^3 particles at $z = 1$, including the power spectrum (PK), correlation function (CF), and bispectrum (BK). In each plot, the top panel shows the clustering measurements of the reference set, the set of paired simulations (non-fixed-amplitude), and the set of paired-fixed-amplitude simulations; the middle panel shows the difference of the mean from each paired set and the reference one divided by the standard deviation from the reference set; the bottom panel shows the ratios of the standard deviations from each paired set and the reference one. From these calculations we can confirm that the suppressed variance method does not introduce significant bias at any scale in the considered range. However, these results show that the improvement depends on the scale. Since the paired

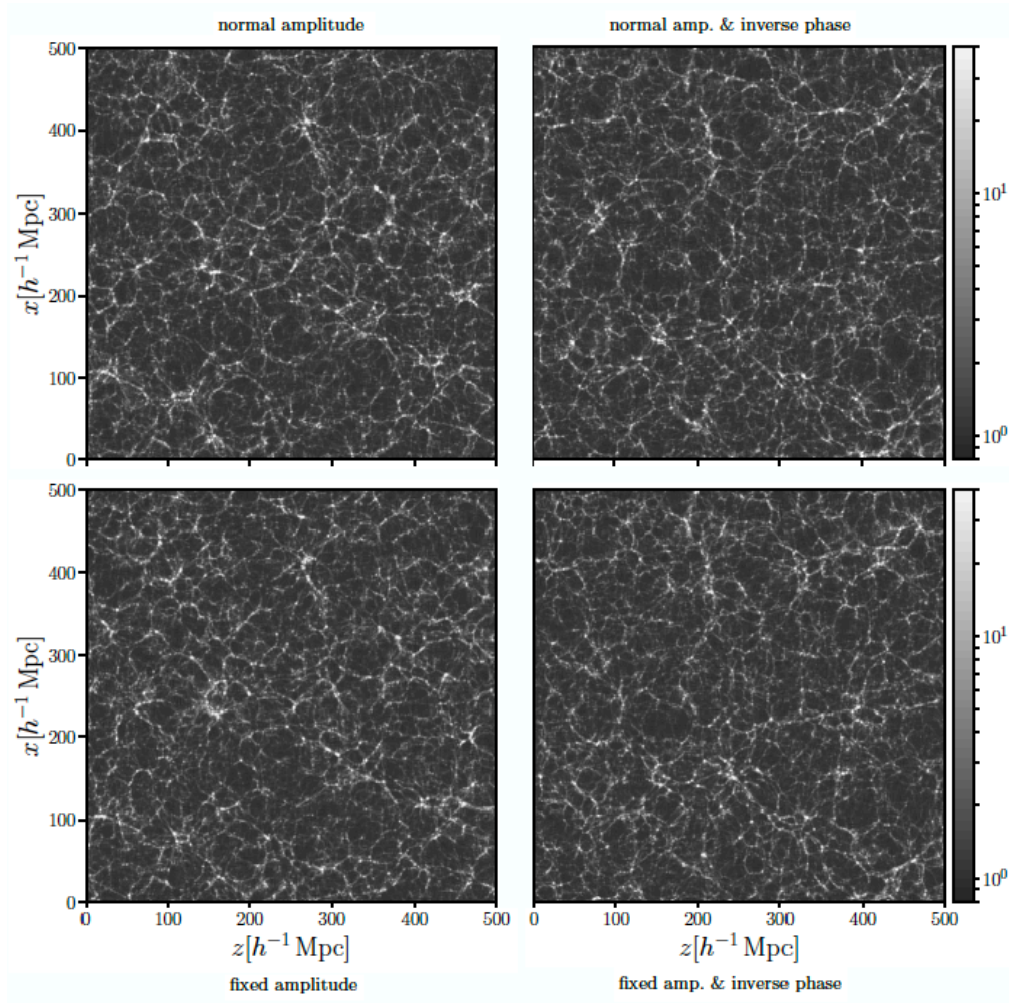


Figure 1. Comparison of regular, fixed amplitude, inverse phases, and combinations, demonstrating on a qualitative level the statistical resemblance between them. Slices of the dark matter density field through the box with $1 h^{-1}\text{Gpc}$ side, which have been zoomed to a $500 \times 500 h^{-1}\text{Mpc}$ region for visualization purposes, corresponding to FastPM simulations with 1024^3 particles at $z = 0$. The panels show the same initial seed perturbations: Regular initial conditions (upper left panel), simulation with inverse phases (upper right panel), simulation with fixed amplitude (lower left panel) and simulation with fixed amplitude and inverse phases (lower right panel).

simulation code	amplitude	phases	box side length	number of particles	particle $M [h^{-1} M_{\odot}]$	force resolution	number of boxes
FastPM A	non-fixed	regular-reference LR	$1 h^{-1}\text{Gpc}$	1024^3	9.6×10^9	$1.46 h^{-1}\text{Mpc}$	100
FastPM \bar{A}	non-fixed	inverse-phase of A	$1 h^{-1}\text{Gpc}$	1024^3	9.6×10^9	$1.46 h^{-1}\text{Mpc}$	100
FastPM B	fixed	regular	$1 h^{-1}\text{Gpc}$	1024^3	9.6×10^9	$1.46 h^{-1}\text{Mpc}$	100
FastPM \bar{B}	fixed	inverse-phase of B	$1 h^{-1}\text{Gpc}$	1024^3	9.6×10^9	$1.46 h^{-1}\text{Mpc}$	100
FastPM C	non-fixed	regular-reference HR	$250 h^{-1}\text{Mpc}$	1024^3	1.2×10^9	$0.36 h^{-1}\text{Mpc}$	100
FastPM \bar{C}	non-fixed	inverse-phase of C	$250 h^{-1}\text{Mpc}$	1024^3	1.2×10^9	$0.36 h^{-1}\text{Mpc}$	100
FastPM D	fixed	regular	$250 h^{-1}\text{Mpc}$	1024^3	1.2×10^9	$0.36 h^{-1}\text{Mpc}$	100
FastPM \bar{D}	fixed	inverse-phase of D	$250 h^{-1}\text{Mpc}$	1024^3	1.2×10^9	$0.36 h^{-1}\text{Mpc}$	100
Gadget G	fixed	regular	$1 h^{-1}\text{Gpc}$	4096^3	1.2×10^9	$6 h^{-1}\text{kpc}$	2
Gadget \bar{G}	fixed	inverse-phase of G	$1 h^{-1}\text{Gpc}$	4096^3	1.2×10^9	$6 h^{-1}\text{kpc}$	2

Table 1. Overview of the set of simulations performed for this study and their corresponding parameter settings, including 800 FastPM and 2 pairs of Gadget simulations. LR and HR refer to low and high resolution, respectively.

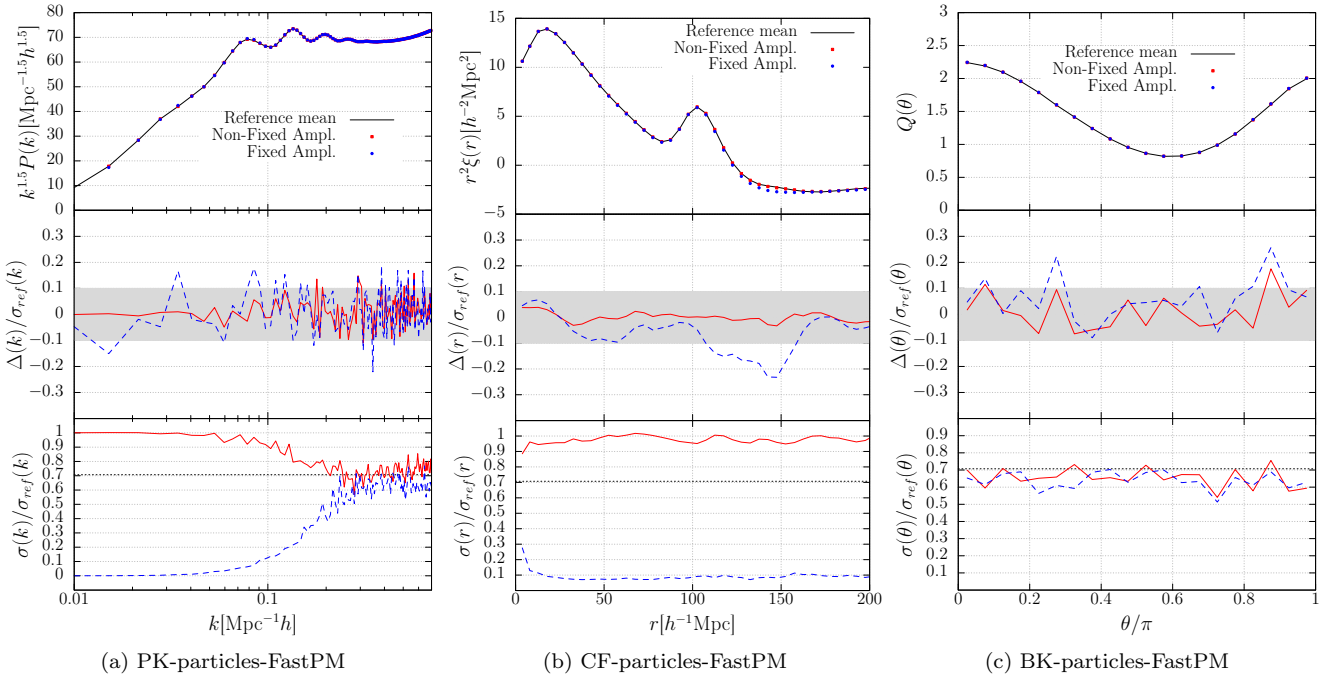


Figure 2. Performance of the Suppressed Variance Method for dark matter particles in real space in the two- (Fourier and configuration space) and three-point statistics. We show the clustering statistics for dark matter particles from FastPM runs with box size $= 1 h^{-1}\text{Gpc}$ and 1024^3 particles at $z = 1$. Left, center, and right panels present the power spectra, correlation functions, and bispectra, respectively. The regular simulation set up is shown in black; the set of paired non-fixed-amplitude simulations in red, and the set of paired-fixed-amplitude simulations in blue. The middle row shows the ratio between $\Delta(k)$ and the standard deviation from the reference LR set. Since the uncertainty on the mean should be inverse proportional to $\sqrt{100}$, deviations between the means should be considered as unbiased if they agree within $0.1\sigma_{\text{ref}}$ (gray region). We confirm that the suppressed variance method does not introduce any statistic significant bias at any scale in the considered range. The correlations among the data points of a correlation function are large at larger scales, so that the deviations shown in the center plot are not statistically significant either. The bottom row shows the ratio between the standard deviations from each paired set, $\sigma(k)$, and the reference LR set, $\sigma_{\text{ref}}(k)$. Since we compare the sets of paired simulation with the reference simulations, if the uncertainty is reduced by only $1/\sqrt{2} \sim 0.7$, it indicates no improvement. We find significant improvement of the uncertainty from the set of paired-fixed-amplitude simulations. However, power spectrum shows that the improvement significantly depends on the scale.

simulations have twice volume of the reference one, there is no improvement if the uncertainty of the paired simulations is larger than or equal to $1/\sqrt{2} \sim 0.7$ of the one measured from the reference simulations. In the case of the power spectrum, we find that the improvement is significant at small k (large scales) but small at large k . If one considers for instance $k > 0.3 h \text{ Mpc}^{-1}$, our results indicate that the variance at large k is dominated by higher-order terms of mode coupling. Interestingly, the improvement in the correlation function variance is nearly constant ($0.1\sigma_{\text{ref}}$) over the range for $r > 10 h^{-1}\text{Mpc}$. We do not find any improvement in the bispectrum with triangle configurations of $k_1 = 0.1$ and $k_2 = 0.2 h \text{ Mpc}^{-1}$. Since we are interested in scales relevant to BAO and RSD analysis, this study goes further into the nonlinear regime as compared to the study of [Angulo & Pontzen \(2016\)](#), in which some improvement was found for the bispectrum in far more linear scales. A deeper study of this can be performed by the community with the data products we provide at this project’s website.

2.2.2 halo catalogs

Our study for halo catalogs shows the same qualitative results as for the dark matter particles, although on a quantitative level the improvement in the suppression of variance is more modest. This is illustrated in Fig. 3, which shows the comparison of the halo clustering measurements, analogous to Fig. 2. From this we conclude that the suppression of variance method is not biased for halo catalogs either at any scale in the considered range. As in the case of dark matter clustering measurements, the improvement in the variance depends on the scale. In this case for the PK and CF at large scales, the ratios of the uncertainties (the bottom panels) can be as small as 0.2 or less which correspond to more than $25 (h^{-1}\text{Mpc})^3$ effectively. Again, for the BK, we do not find any improvement.

The halo population is represented by a fraction of all dark matter particles. It is sensitive to small-scale fluctuations in the initial density field, affecting the mass and location of gravitational collapse. This effect is many times referred to as stochasticity and explains the difference in the results with respect to the dark matter particles performance.

The results for redshift-space halo clustering including

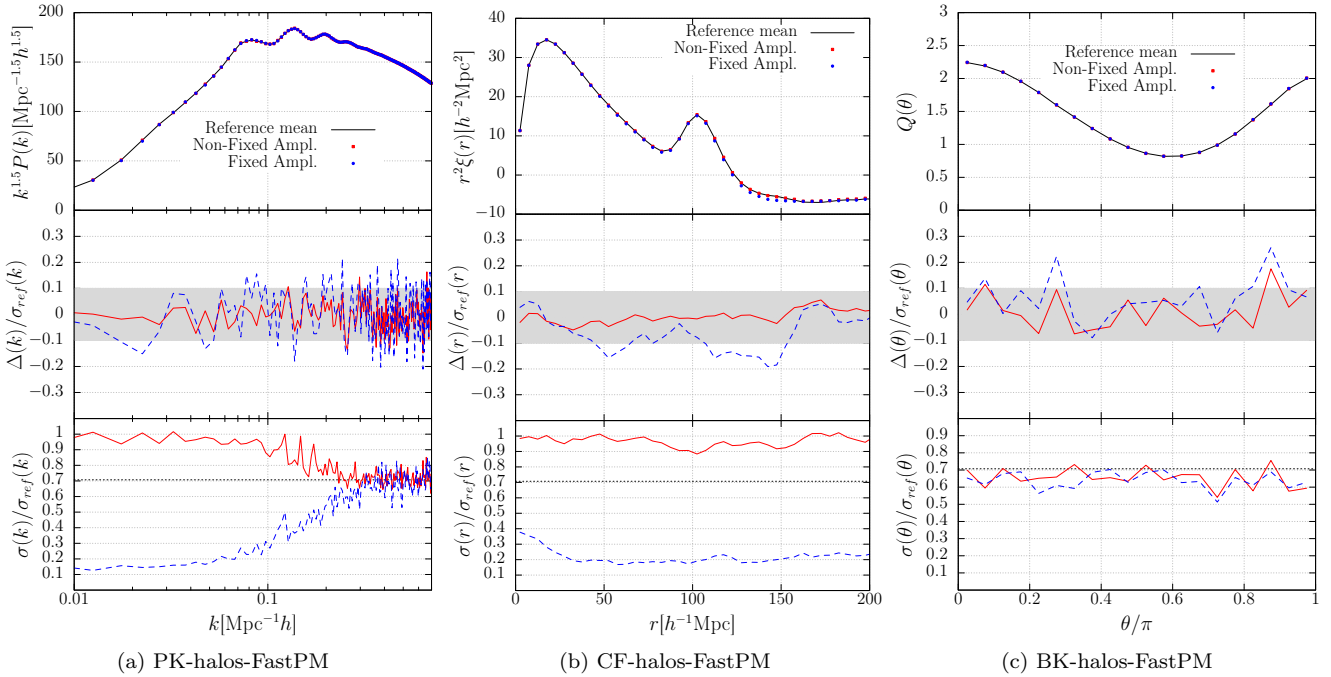


Figure 3. Performance of the Suppressed Variance Method for the halo catalog in real space in the two- (Fourier and configuration space) and three-point statistics. Same as in Fig. 2, but for halos. We do not find any bias in these measurements (see the middle panels). The improvements in the uncertainties are weaker than the ones from dark matter clustering measurements but are still significant. There is no improvement in the power spectrum for $k > 0.3 \text{Mpc}^{-1} h$ at $z = 1$.

monopoles and quadrupoles in configuration and Fourier space show a similar performance to the real-space measurements, as can be seen in Fig. 4. We use the same definition of the multipole expansion as in Chuang et al. (2017).

2.2.3 halo mass function

As another relevant statistic, we investigate the halo mass function, shown for $z = 1$ in Fig. 5. We find no bias in the mean, and only a slight improvement in the variance below a mass of approximately $M < 10^{13} h^{-1} M_{\odot}$. We further check this in the additional set of FastPM boxes with smaller box size but higher resolution and confirm the improvement of the mass function in the lower mass bins. Further tests are shown at <http://www.unitsims.org>. In that supplementary material we also show that the suppression of variance is more effective a) towards increasing redshifts, as structure formation becomes more linear; and b) for lower mass cuts, as the higher mass populations suffer more from stochasticity (see also Section 3 for another representation of these trends).

2.2.4 void clustering

We now consider cosmic voids. We focus on the well-defined convention used in the void finder code DIVE (Zhao et al. 2016), which considers voids as empty spheres constrained by quartets of galaxies. This definition has proved useful to study the troughs of the density field, i.e. the clustering within cosmic voids, and to obtain improved measurements of the BAO signature (see Kitaura et al. 2016; Liang

et al. 2016; Zhao et al. 2018). Cosmic voids in fact are measures of the higher-order statistics of the galaxy distribution (see above mentioned papers and references therein), and are therefore interesting to study the performance of suppressed variance methods. As expected from the BK result, the auto-correlation function of the voids, shown in Fig. 6, shows a very moderate improvement in the uncertainty and no bias. However, the cross-correlation functions between halos and voids present significant improvements, shown in Fig. 7.

3 APPLICATION OF SVM FOR CLUSTERING ANALYSIS FROM GALAXY SURVEYS

We have demonstrated in the previous section that the suppressed variance method does not introduce any bias, and significantly reduces the uncertainty in the two-point statistics. We now proceed to produce our first two pairs of high-resolution full N -body simulations aimed at the analysis of ELG and LRG data from DESI- and Euclid-like surveys.

3.1 Setup

We use the N -body code GADGET (Springel 2005), a full MPI parallel code that uses the Particle-Mesh (PM) + Tree algorithms to compute the Newtonian forces between the dark matter particles by splitting the gravitational force into a long-range term (computed through the PM method) and a short-range term taken from the nearest neighbors, using a Tree method to categorize the particles according to their relative distances.

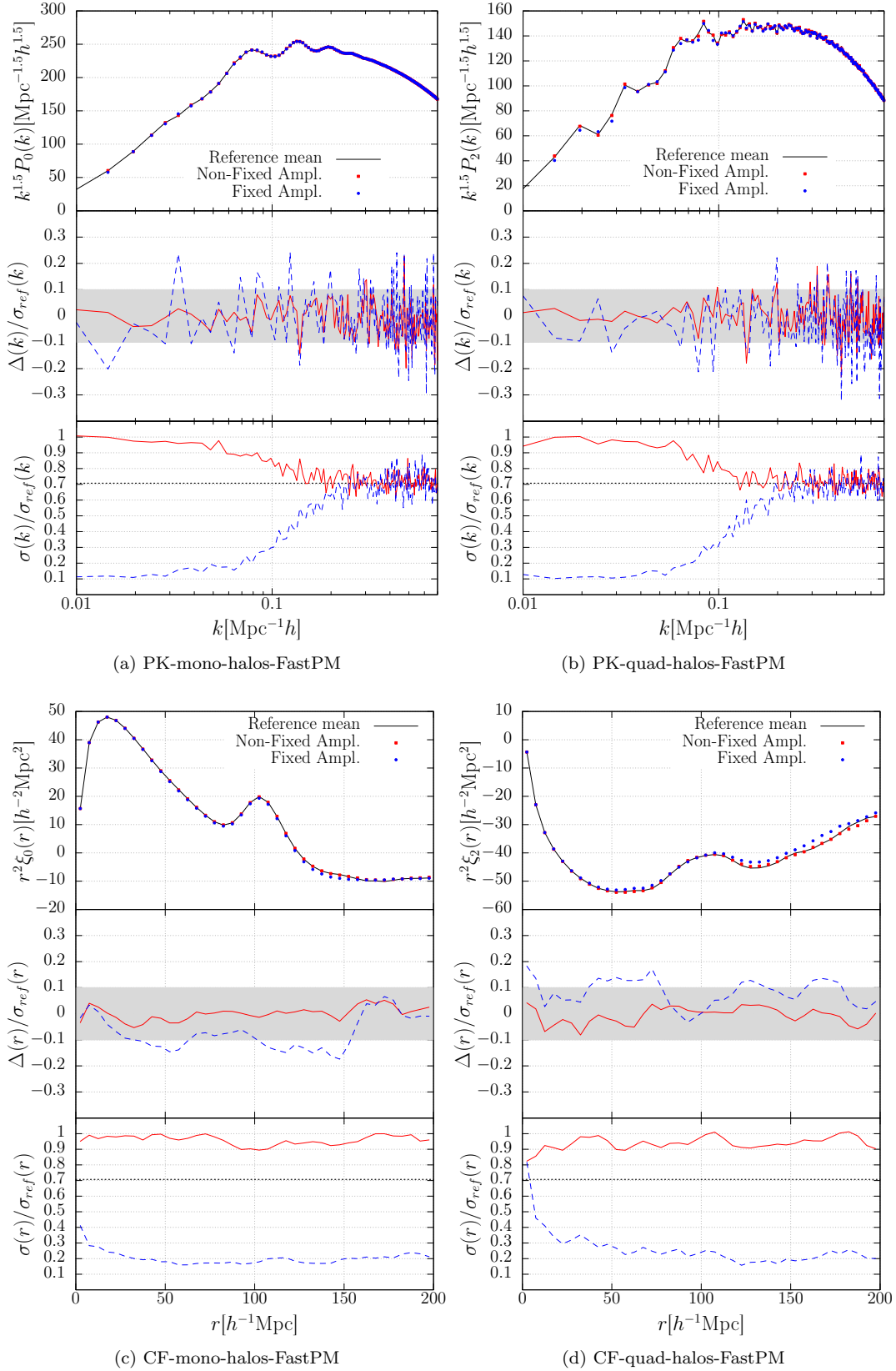


Figure 4. Performance of the Suppressed Variance Method for the halo catalog in redshift space in the monopole and quadrupole (Fourier and configuration space). The panels show the monopole (left panels) and the quadrupole (right panels) in Fourier space (top set) and configuration space (bottom set). The same conventions as in Fig. 3 are used. We do not find any bias in these measurements. The improvements are similar to those found in real space.

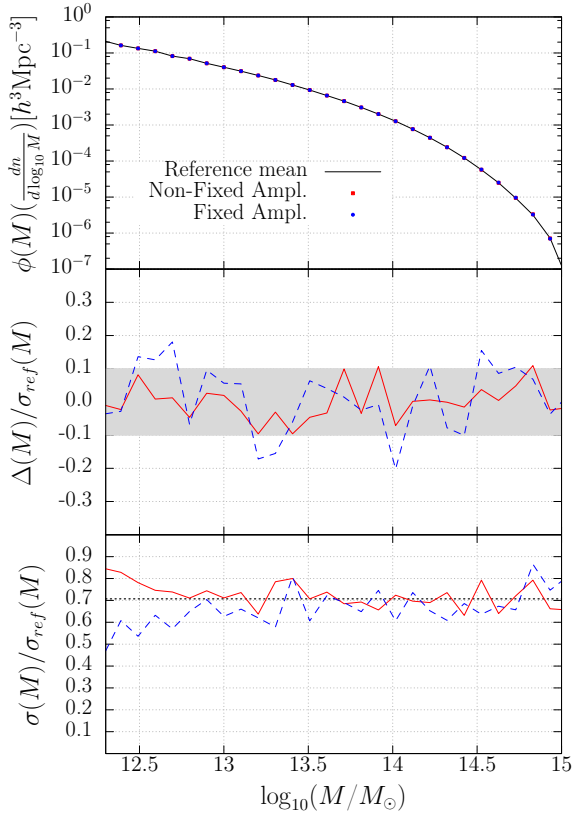


Figure 5. Halo mass functions with same conventions as in Fig. 2. We find no bias in the mean. We find a slight improvement in the variance below a mass of approximately $M < 10^{13} h^{-1} M_{\odot}$.

This code makes use of the public software library FFTW for parallel Fast-Fourier transforms and the GNU Scientific Library (GSL). We are using a non-public version of the code, named L-GADGET, which is highly optimized for large-volume simulations with a cubic domain decomposition and an efficient use of internal memory. This code has been extensively used to produce large-volume simulations with hundreds of billions of particles. The same code has also been used to produce other large simulations like the Multidark simulation suite (see <http://www.multidark.org>) and the Millenium series of simulations (including the Millenium XXL with more than 300 billion particles).

The paired initial conditions with fixed amplitude are generated within second order Lagrangian perturbation theory with FastPM (Feng et al. 2016). We use the same cosmology as the FastPM simulations generated for this study (see Section 2). The box size is $1 h^{-1} \text{Gpc}$ and the simulation is started at $a \equiv 1/(1+z) = 0.01$ ($z = 99$). The number of particles is 4096^3 , giving a particle mass is $\sim 1.2 \times 10^9 h^{-1} M_{\odot}$. We use the halo finder code ROCKSTAR (Behroozi et al. 2013a) to identify haloes and compute their merging histories using the CONSISTENT TREES software (Behroozi et al. 2013b).

3.2 Results from full N -body simulations

The resolution of our large full N -body simulations has been chosen to match the resolution of our small-volume particle mesh simulations using the FastPM code. The halo catalogs were generated using a minimum halo mass of 1.2×10^{11}

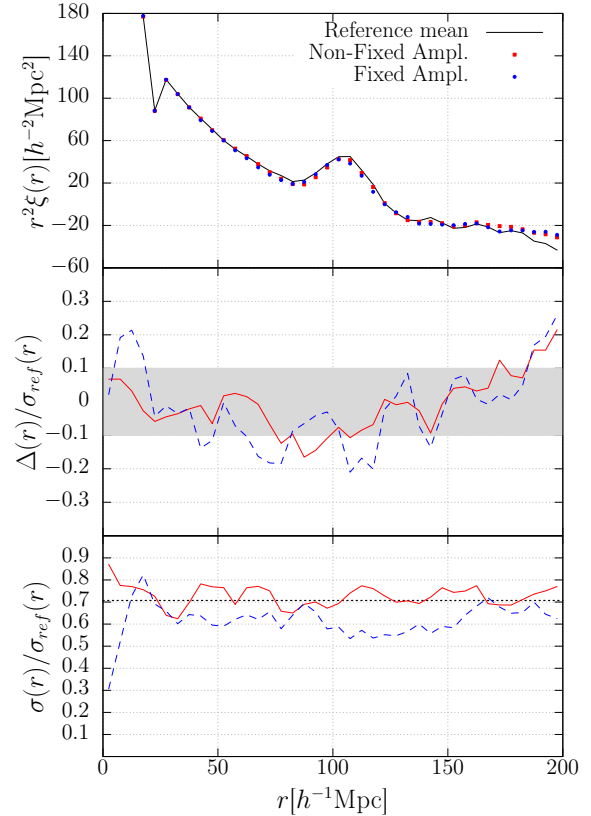


Figure 6. Void auto-correlation function selected with the radius cut $12 h^{-1} \text{Mpc}$ using the DIVE code with same conventions as in Fig. 2. It shows a very moderate improvement in the uncertainty and no bias.

$h^{-1} M_{\odot}$ (at this limit the mass function is quite complete, as shown in the right-most panel of Fig. 8). This permits us to assess the improvement in the statistics from the FastPM simulations with the $250 h^{-1} \text{Mpc}$ box size and a mesh of 1024^3 . We show the power spectrum, correlation function, and halo mass function measurements from our fixed-amplitude-paired Gadget N -body simulations in Fig. 8, which turn out to be remarkably smooth for the different redshift snapshots. We explore robust statistical measures in the next section to further assess the quality of the simulations.

3.2.1 Estimator quantifying the improvement in SVM

Thus far, we have shown the improvements at different scales for different clustering statistics. However, in a practical cosmological analysis (see e.g. Chuang et al. 2017), we use a specific scale range (e.g. $40 < r < 200 h^{-1} \text{Mpc}$ in configuration space or $0.02 < k < 0.2 h \text{Mpc}^{-1}$ in Fourier space), so the improvement should be determined by the whole range. To quantitatively assess the improvement, we adopt the Fisher information matrix formalism evaluating the improvement of the constraining power on a given cosmological parameter by performing the analysis within a certain scale range. In this approach, the uncertainty of a given cosmological

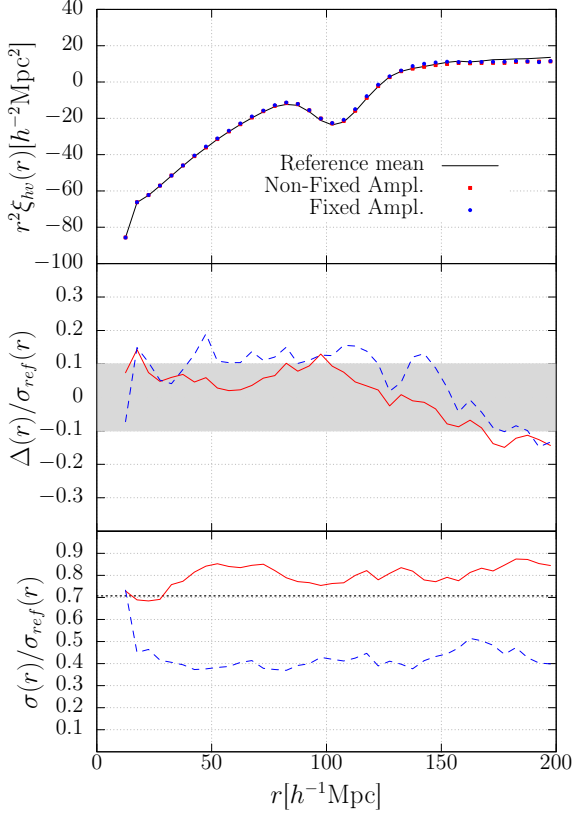


Figure 7. Same as Fig. 6, but for void-galaxy cross-correlation function. This shows significant improvement in the prediction, compared to the void auto-correlation function.

parameter (θ) is defined as

$$\text{Var}(\theta) = (F^{-1})_{\theta,\theta} \quad (1)$$

$$= \left\langle \frac{-\partial^2 \ln P(\theta)}{\partial \theta^2} \right\rangle^{-1} \quad (2)$$

$$\propto \left\langle -\frac{\partial^2 \left(\text{Tr}[\log C] + \sum_{ij} f_i \text{Tr} C_{ij}^{-1} f_j \right)}{\partial \theta^2} \right\rangle^{-1} \quad (3)$$

$$(4)$$

where $P(\theta)$ is the posterior, and $\langle \dots \rangle$ denotes the expectation value. C is the covariance matrix of some measurement f (e.g. PK or CF), and i, j are the indices of the elements, i.e. $C_{ij} = \langle f_i f_j \rangle$ (Dodelson 2003). We have assumed a flat prior on the parameter θ and a Gaussian likelihood. For simplicity, we further assume that all the measured data points within the scale range of interest have the same sensitivity to the parameter θ , i.e. $\partial f_i / \partial \theta = \partial f_j / \partial \theta$, $\forall i, j$. With these assumptions, the uncertainty of the parameter θ can be related to the covariance matrix of the data vector via the following equation,

$$\text{Var}(\theta) = A \left(\sum_{i,j} (C^{-1})_{ij} \right)^{-1}, \quad (5)$$

where i, j go through all the data points within the scale range of interest, and A is assumed to be a constant involving terms $(\partial f / \partial \theta)^2$.

We then quantify the covariance matrix of the data vector from the simulation. We note that in order to perform the cosmological analysis, one has to account for two types of uncertainties. The first one is the theoretical uncertainty, represented by the theoretical covariance, C_{theo} , which is driven by the statistics variance of the simulations used to validate the models. The second one is the observational uncertainties encoded in the covariance matrix C_{obs} . For a galaxy survey, for example, this would include sample variance on large scales, and stochasticity on small scales. The total covariance matrix is given by the sum of the individual ones, i.e.

$$C = C_{\text{theo}} + C_{\text{obs}}. \quad (6)$$

The reasonable assumption here is that there are no cross-covariances between the two.

The theoretical covariance matrix, C_{theo} , can be calculated from the simulations used for validating the models with either the fixed amplitude or the regular N -body simulations. We will quantify the difference between these two choices below. We first estimate the observational covariance matrix, C_{obs} , by rescaling the covariance matrix from the regular simulations based on the expected survey volume. Consider an effective volume of $20 (h^{-1} \text{Gpc})^3$, roughly corresponding to that of the DESI and Euclid surveys. The covariance matrix including a pair of fixed-amplitude simulations can be computed by

$$C = C_{\text{SVM}} + \frac{C_1}{V_{\text{EFFS}}}, \quad (7)$$

where C_1 is the covariance matrix of a single regular $1 (h^{-1} \text{Gpc})^3$ box, V_{EFFS} is the effective survey volume ($20 (h^{-1} \text{Gpc})^3$ in our study), and C_{SVM} is the covariance matrix of the suppressed variance method (paired fixed amplitude simulation). Following Equation 5, we compute the variance, Var_{SVM} .

Let us now answer the question: What is the size of the required standard simulation, that yields the equivalent variance of a pair of simulations with the SVM? Given a normal simulation with volume $V = (h^{-1} \text{Gpc})^3$, the total covariance matrix is given by

$$C_V = \frac{C_1}{V} + \frac{C_1}{V_{\text{EFFS}}}. \quad (8)$$

We now compute the variance Var_V based on 5. By solving $\text{Var}_{\text{SVM}} = \text{Var}_V$, we obtain the equivalent volume (V) that our paired fixed amplitude simulations are representing. This is shown in Fig. 9; the equivalent volume vs. scale ranges used in the power spectrum and correlation function analysis are shown. Here the maximum separation was fixed and the minimum separation was varied in the correlation function analysis; while the minimum k was fixed and the maximum k was varied in the power spectrum analysis.

We find that a pair of $1 (h^{-1} \text{Gpc})^3$ boxes can potentially correspond to effective volumes of up to $100 (h^{-1} \text{Gpc})^3$ considering halos with lower masses. We also find that the equivalent volume is sensitive to the power spectrum, but not to the correlation function analysis. One might obtain very large effective volumes by ignoring the covariance matrix from observations, artificially driven by the uncertainty at large scales (e.g. small k). Thus, this additional covariance matrix needs to be taken into account, as we do in our analysis.

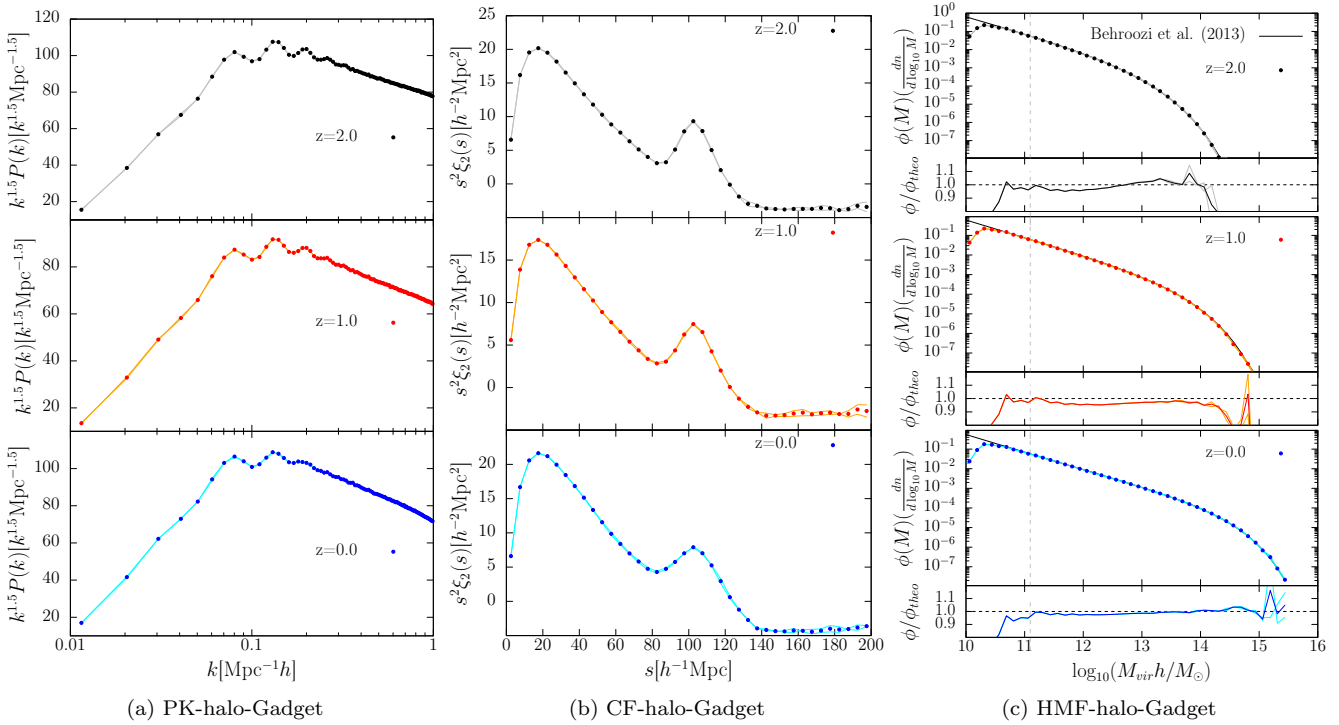


Figure 8. Power spectrum, correlation function, and halo mass function measurements from full N -body simulations with the SVM. SVM reduces the variances significantly so that the measurements are very smooth.

Interestingly, the naive correspondence between $k \sim 0.35 h\text{Mpc}^{-1}$ and $r \sim 20 h^{-1}\text{Mpc}$ using $k = 2\pi/L$, yields completely different effective volumes: roughly 10 and 100 $(h^{-1}\text{Gpc})^3$, respectively (see lower panels in Fig. 9). This is emphasizing the difference in the Fourier and configuration space analysis, when a limited range in k or r is used.

In contrast to configuration space, Fourier space turns out to be more sensitive towards large scales (low k s), which are apparently already linear (say $k \sim 0.2 h\text{Mpc}^{-1}$). The reason is that the fixed power spectrum step is crucial to reduce the variance, as we showed in detail in Section 2.1, but does not solve nonlinear gravitational mode-coupling. This is very apparent in Fourier space analysis. We can find analogous examples in the literature comparing the two-point statistics in Fourier and configuration space, such as 1) aliasing introduced by the gridding process of a set of point sources onto a mesh (Hockney & Eastwood 1988), in which a clouds-in-cells mass assignment scheme applied on dark matter particles in a cosmological simulation with cell resolutions of a few Mpc scales, underestimates the true power spectrum down to $k \sim 0.2 h\text{Mpc}^{-1}$ (Jing 2005); 2) or in the clustering analysis of galaxies in redshift space, in which the virialised motions (a.k.a. fingers-of-god, Jackson 1972) are well constrained below a certain scale (of ~ 20 Mpc), but are visible down to $k \sim 0.1 h\text{Mpc}^{-1}$ in Fourier space. This is also indicating that pairing simulations with opposite phases is not being very successful at suppressing the variance at small scales, as we already saw in the three-point statistics analysis (see Section 2.1) and further improvements should be investigated.

We conclude from this analysis, that our two pairs of high resolved N -body simulations with the SVM have an

effective volume larger than 7 times of the DESI or Euclid effective survey volumes when the analysis is performed in configuration space. We are currently preparing larger sets of SVM N -body simulations to ensure that this accuracy is also achieved in Fourier space.

4 SUMMARY AND CONCLUSIONS

In this work we have presented the UNIT N -body cosmological simulation project and its corresponding data products, including dark matter particles, halo catalogs, and clustering statistics. We show that the effective volume of our simulation suite is equivalent to $150 (h^{-1} \text{Mpc})^3$ (7 times of the effective survey volume of DESI or Euclid), using a mass resolution of $\sim 1.2 \times 10^9 h^{-1} M_{\odot}$, enough to resolve the host halos of the galaxy sample observed by DESI (ELGs) or Euclid (H α galaxies).

Our work relies on the suppressed variance method (SVM) approach recently introduced by Angulo & Pontzen (2016). In order to demonstrate the practicality of the SVM for large-scale structure analyses, we investigate a number of issues including potential biases introduced by the method, and characterize the improvement in the theoretical uncertainty / effective volume in a number of different regimes.

We have performed a large number (800) of accurate particle mesh simulations using the FastPM code, and have demonstrated that no significant biases are introduced that could affect BAO or RSD analysis. We found that the error is greatly reduced in two-point statistics. No significant improvement is found for the three-point statistics on scales relevant to BAO and RSD analysis. We also performed

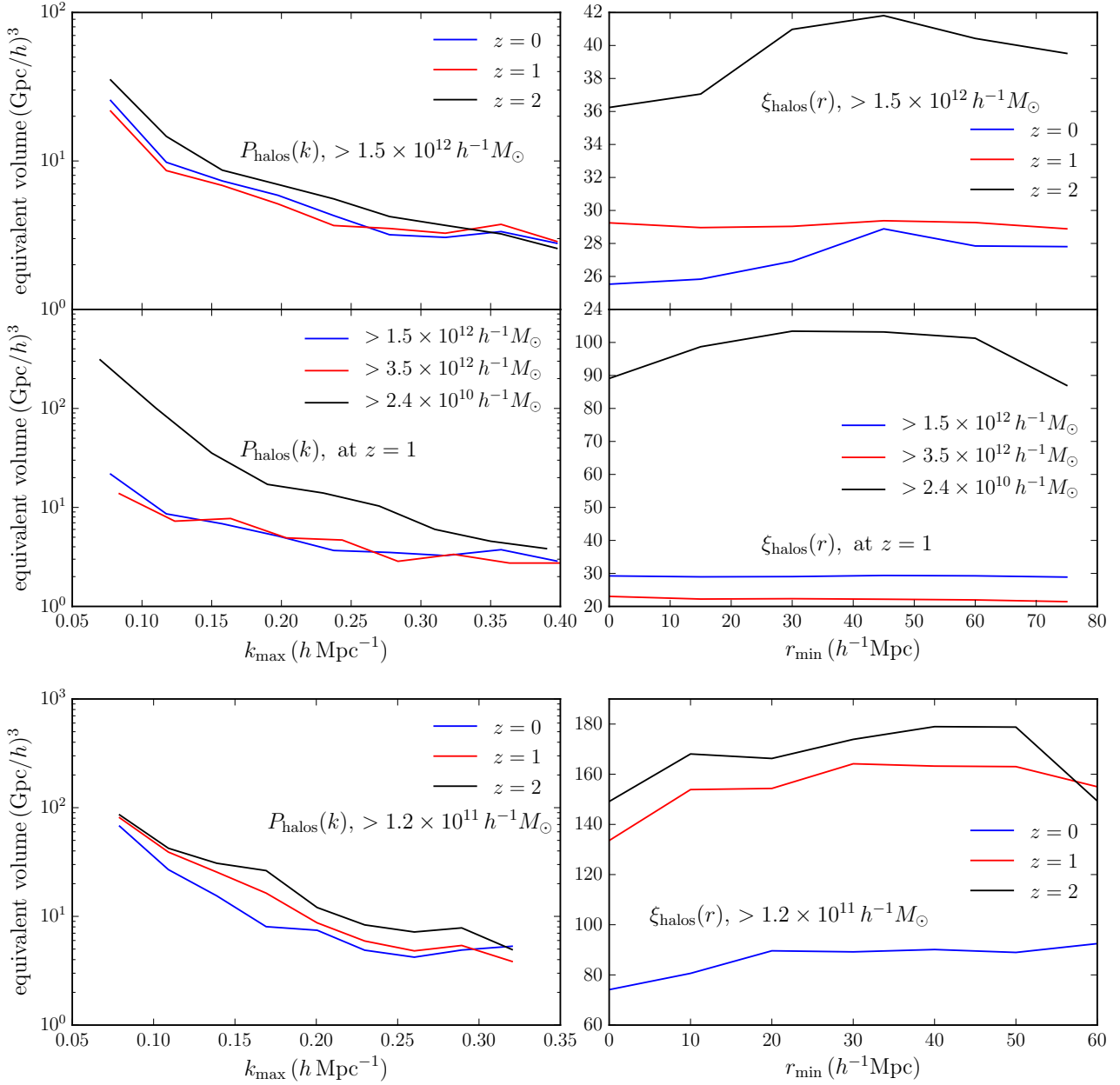


Figure 9. Equivalent volume study of the SVM for different redshifts and mass cuts. The upper four panels show the equivalent volumes of the catalogues from one pair of $1 h^{-1}\text{Gpc}$ boxes. The low two panels show the equivalent volumes of the catalogues from two pairs of $1 h^{-1}\text{Gpc}$ boxes which are corresponding to our high resolution full N -body simulations. The results shown in the left are in Fourier space (varying k_{max} with fixed $k_{\text{min}} = 0$) and in the right are in configuration space (varying r_{min} with fixed $r_{\text{max}} = 120$).

an analysis including redshift-space distortions, and three-dimensional halo distributions beyond the halo mass function.

We introduced a parameter for quantifying the improvement of the suppressed variance methods, and show that these simulations are equivalent to a typical simulation with volume of $100 (h^{-1} \text{Gpc})^3$. The exact number depends on both the analysis method considered and the galaxy sample used.

We found that the improvements in galaxy bispectrum and void auto-correlation function using SVM are small. However, the improvement in the void-galaxy cross-

correlation is significant; this indicates that the fixed-amplitude method should also be useful for some void studies.

With current state-of-the-art techniques we found that for a galaxy survey with effective volume of $20 (h^{-1} \text{Gpc})^3$, the gain is about a factor of 40. This means that our two pairs of simulations with full N -body calculations with volumes of $(1 h^{-1} \text{Gpc})^3$ and 4096^3 particles lead to the same variance as ~ 150 of such simulations. This provides optimal reference clustering measurements to validate theoretical models in configuration space. The improvement is more moderate in Fourier space, but is still significant. This mo-

tivates future work to compute larger sets of N -body simulations using SVM. We are pursuing this, as well as further analysis to investigate mode-coupling effects from larger scales and ways of correcting them.

In the spirit of sharing scientific results with the community, we have made the full N -body simulations in addition to the FastPM products produced in this work publicly available through the website <http://www.unitsims.org>. We hope that these data products will enable a number of studies to further unveil the nature of dark energy and structure formation with galaxy surveys.

ACKNOWLEDGEMENTS

We thank Raul E. Angulo, Elena Massara, and Andrew Pontzen for useful discussions, and Volker Springel for providing the L-Gadget code. We acknowledge PRACE for awarding us access to the MareNostrum Supercomputer hosted by the Barcelona Supercomputing Center, Spain, under project grant number 2016163937. GY and AK would like to thank MINECO/FEDER (Spain) for partial financial support under project grant AYA2015-63810P. AK further thanks the Spanish Red Consolider MultiDark FPA2017-90566-REDC. FSK thanks support from the grants RYC2015-18693, SEV-2015-0548, and AYA2017-89891-P. CZ thanks support under NSFC Grant No. 11673025. SA is supported by the European Research Council through the COSFORM Research Grant (#670193). This research received support from the U.S. Department of Energy under contract number DE-AC02-76SF00515, Additional computing support was provided by SLAC and by National Energy Research Scientific Computing Center (NERSC), a U.S. Department of Energy Office of Science User Facility operated under Contract No. DE-AC02-05CH11231.

REFERENCES

- Abell P. A., et al., 2009, preprint ([arXiv:0912.0201](https://arxiv.org/abs/0912.0201))
- Angulo R. E., Pontzen A., 2016, *MNRAS*, 462, L1
- Angulo R. E., Springel V., White S. D. M., Jenkins A., Baugh C. M., Frenk C. S., 2012, *MNRAS*, 426, 2046
- Behroozi P. S., Wechsler R. H., Wu H.-Y., 2013a, *ApJ*, 762, 109
- Behroozi P. S., Wechsler R. H., Wu H.-Y., Busha M. T., Klypin A. A., Primack J. R., 2013b, *ApJ*, 763, 18
- Benitez N., et al., 2014, preprint ([arXiv:1403.5237](https://arxiv.org/abs/1403.5237))
- Chuang C.-H., et al., 2017, *MNRAS*, 471, 2370
- Cochrane R. K., Best P. N., Sobral D., Smail I., Wake D. A., Stott J. P., Geach J. E., 2017, *MNRAS*, 469, 2913
- Dodelson S., 2003, *Modern cosmology*. Academic Press
- Feng Y., Chu M.-Y., Seljak U., McDonald P., 2016, *MNRAS*, 463, 2273
- Fosalba P., Crocce M., Gaztañaga E., Castander F. J., 2015, *MNRAS*, 448, 2987
- González-Pérez V., et al., 2018, *MNRAS*, 474, 4024
- Habib S., et al., 2016, *New Astron.*, 42, 49
- Hand N., Feng Y., Beutler F., Li Y., Modi C., Seljak U., Slepian Z., 2017, preprint ([arXiv:1712.05834](https://arxiv.org/abs/1712.05834))
- Hill G., Gebhardt K., Komatsu E., Drory N., MacQueen P., et al., 2008, *ASP Conf. Ser.*, 399, 115
- Hockney R. W., Eastwood J. W., 1988, *Computer simulation using particles*
- Jackson J. C., 1972, *MNRAS*, 156, 1P
- Jing Y. P., 2005, *ApJ*, 620, 559
- Kitaura F.-S., et al., 2016, *Phys.Rev.Lett.*, 116, 171301
- Klypin A., Prada F., 2018, preprint ([arXiv:1809.03637](https://arxiv.org/abs/1809.03637))
- Klypin A., Yepes G., Gottlober S., Prada F., Hess S., 2016, *MNRAS*, 457, 4340
- Laureijs R., et al., 2011, preprint ([arXiv:1110.3193](https://arxiv.org/abs/1110.3193))
- Levi M., et al., 2013, preprint ([arXiv:1308.0847](https://arxiv.org/abs/1308.0847))
- Liang Y., Zhao C., Chuang C.-H., Kitaura F.-S., Tao C., 2016, *MNRAS*, 459, 4020
- Planck Collaboration XIII et al., 2016, *A&A*, 594, A13
- Pontzen A., Slosar A., Roth N., Peiris H. V., 2016, *Phys.Rev.*, D93, 103519
- Potter D., Stadel J., Teyssier R., 2016, preprint ([arXiv:1609.08621](https://arxiv.org/abs/1609.08621))
- Schlegel D., et al., 2011, preprint ([arXiv:1106.1706](https://arxiv.org/abs/1106.1706))
- Skillman S. W., Warren M. S., Turk M. J., Wechsler R. H., Holz D. E., Sutter P. M., 2014
- Spergel D., et al., 2013, preprint ([arXiv:1305.5422](https://arxiv.org/abs/1305.5422))
- Springel V., 2005, *MNRAS*, 364, 1105
- Takada M., et al., 2014, *PASJ*, 66, R1
- Tassev S., Zaldarriaga M., Eisenstein D., 2013, *JCAP*, 1306, 036
- Villaescusa-Navarro F., et al., 2018, preprint ([arXiv:1806.01871](https://arxiv.org/abs/1806.01871))
- White M., 2015, *MNRAS*, 450, 3822
- Zel'dovich Y. B., 1970, *A&A*, 5, 84
- Zhao C., Tao C., Liang Y., Kitaura F.-S., Chuang C.-H., 2016, *MNRAS*, 459, 2670
- Zhao C., Chuang C.-H., Liang Y., Kitaura F.-S., Vargas-Magaña M., Tao C., Pellejero-Ibanez M., Yepes G., 2018, preprint ([arXiv:1802.03990](https://arxiv.org/abs/1802.03990))
- de Jong R. S., Bellido-Tirado O., Chiappini C., Depagne E., Haynes R., et al., 2012, preprint ([arXiv:1206.6885](https://arxiv.org/abs/1206.6885))

This paper has been typeset from a $\text{\TeX}/\text{\LaTeX}$ file prepared by the author.